Title

Ambient pressure XPS and IRRAS investigation of ethanol steam reforming on Ni—CeO 2 (111) catalysts: an in situ study of C—C and O—H bond scission

Journal

Physical Chemistry Chemical Physics, 18(25)

ISSN

0956-5000

Authors

Liu, Zongyuan
Duchoň, Tomáš
Wang, Huanru
et al.

Publication Date

2016-06-22

DOI

10.1039/c6cp01212d

Peer reviewed

Ambient pressure XPS and IRRAS investigation of ethanol steam reforming on Ni-CeO2(111) catalysts: an in-situ study of C-C and O-H bond scission

Zongyuan Liu [†,ʃ], Tomáš Duchoň [‡], Huanru Wang [ʃ], David C. Grinter [ʃ], Iradwikanari Waluyo [ʃ], Jing Zhou [δ], Qiang Liu [#], Beomgyun Jeong [#], Ethan Crumlin [#], Vladimír Matolín [‡], Dario J. Stacchiola [ʃ], José A. Rodriguez [†,ʃ], Sanjaya D. Senanayake [ʃ,]*

[†] Department of Chemistry, Stony Brook University, Stony Brook, NY, 11794

[ʃ] Chemistry Department, Brookhaven National Laboratory, Upton, New York 11973

[‡] Faculty of Mathematics and Physics, Charles University in Prague, V Holešovičkách 2, Praha 8, Czech Republic

[δ] Department of Chemistry, University of Wyoming, Laramine, WY 82071

[#] Advanced Light Source, Lawrence Berkeley National Laboratory, Berkeley, CA 94720

[*] Corresponding author: Bldg. 555A, Brookhaven National Lab, P.O. Box 5000, Upton, NY 11973-5000, 631-344-4343, ssenanay@bnl.gov

Abstract

Ambient-Pressure X-ray Photoelectron Spectroscopy (AP-XPS) and Infrared Reflection Absorption Spectroscopy (AP-IRRAS) have been used to elucidate the active sites and mechanistic steps associated with the ethanol steam reforming reaction (ESR) over Ni-CeO_2(111) model catalysts. Our results reveal that surface layers of the ceria substrate are both highly reduced and hydroxylated under reaction conditions while the small supported Ni nanoparticles are present as Ni^0/Ni_xC. A multifunctional, synergistic role is highlighted in which Ni, CeO_x and the interface provide an ensemble effect in the active chemistry that leads to H_2. Ni^0 is the active phase leading to both C-C and C-H bond cleavage in ethanol but it is also responsible for carbon accumulation or coking. On the other hand, CeO_x is important for the adsorption of ethanol and H_2O, followed by the deprotonation to ethoxy and OH intermediates. The active state of CeO_x is a $Ce^{3+}(OH)_x$ compound, that results from extensive reduction by ethanol and the efficient dissociation of water. The interface (Ni-ceria) facilitates the C-C bond breaking step while the pathways that lead to H_2 production may occur from the recombination of OH and CH_x species. Additionally, we discuss an important insight into the stability and selectivity of the catalyst in the presence of water, where the accumulation of surface carbon can be mitigated by the increased presence of surface OH groups. We propose the co-existence and cooperative interplay of Ni^0 and $Ce^{3+}(OH)_x$, in the activation of ethanol/water as well as in the removal of coke, through a metal-support interaction facilitates oxygen transfer and the efficient extraction of H_2.

TOC

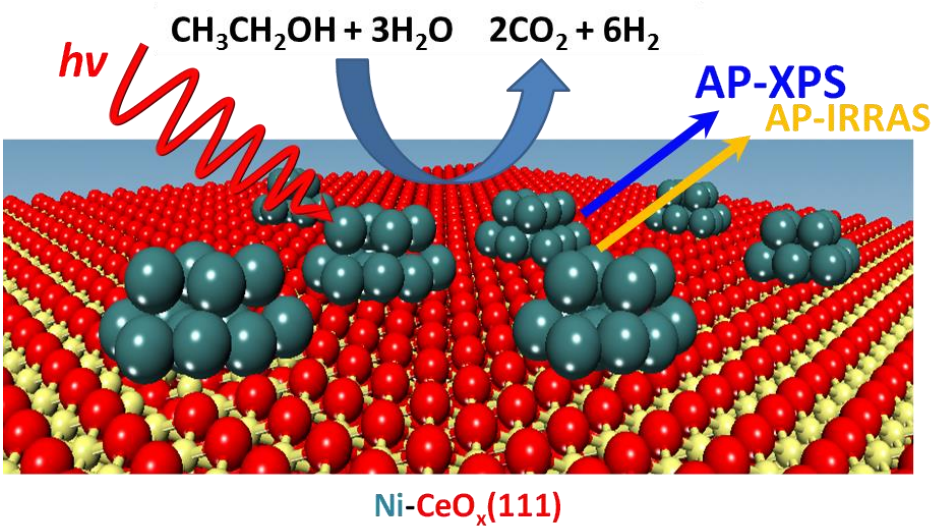

Keywords: Ethanol, Steam reforming, H_2 production, Ceria, Nickel, AP-XPS, IRRAS.

INTRODUCTION

Traditionally, the steam reforming of ethanol (ESR: $C_2H_5OH + 3\ H_2O \rightarrow 6\ H_2 + 2\ CO_2$) is an important process in the chemical industry, while more recently it is being employed in fuel cell applications, where it provides an alternative route to obtain renewable hydrogen through the reforming of hydrocarbon oxygenates (eg. bio-ethanol), from sustainable sources such as biomass.[1-2] Metal supported oxide catalysts have shown significant activity for this reaction.[1, 3-15] Notably, Ni-oxide based materials have emerged as promising catalysts for the ESR reaction and have been reported to exhibit activity and/or selectivity comparable to that of expensive noble metals such as Rh, Pt and Pd.[16-18]

The behavior of ceria supported nickel nanoparticles is quite different from that of bulk Ni, a system which is very active for CO methanation and undergoes rapid deactivation by coke formation during the steam reforming process.[8, 16, 19] Ni and ceria, when combined in the same catalyst, have the ability to activate both ethanol (C-C and C-H bonds) and H_2O (O-H), and selectively extract H_2, without the production of CH_4 or other C-O byproducts (aldehydes or olefins) provided certain phenomenological factors are maintained. This includes compositional, geometric and morphological effects of keeping Ni loading low, small in size, well dispersed and in good contact with ceria.

Both experimental and DFT calculations results suggest that the small Ni nanoparticles on CeO_2(111) are activated, electronically perturbed and can thus influence catalytic chemistry through metal-support interactions.[16, 20-21] Hydroxyl groups generated from these strong metal-support interactions could play an important role in redox chemistry such as in the water-gas shift (WGS) reaction and for suppressing coke formation with subsequent deactivation.[21]

We have previously studied Ni and CeO_x based systems as powder catalysts and identified them as active for the ESR reaction, and we also adopted strategies for protecting the active Ni centers in solid solutions of the $Ni_xCe_yO_z$ type.[8, 16] We attributed the sustained activity and good stability to the suppression of sintering under harsh reaction conditions, which leads to the sustained contact between Ni and CeO_x and the prevention of coking. Furthermore, previous studies by Duhamel et al. of hydrogenated Ni-ceria powder catalysts proposed that hydroxyls played a key role as interfacial stabilizers and thus aid in keeping the metal and oxide in contact through an active Ni-OH-CeO_x phase that significantly improved the catalytic activity and stability.[22-23] However, no studies have been able to unequivocally confirm this process, and obtain an *in situ* surface sensitive perspective into the role of hydroxyl groups on the formation of C-intermediates and the removal of coke. We present here the very first instance of the use of ambient pressure photoelectron spectroscopy (AP-XPS) and Infrared Reflection Absorption Spectroscopy (IRRAS) to identify the catalytic chemistry under steady state reaction conditions (40-300 mTorr). We have strived to gain insights into the elementary steps of how water and ethanol reacts, specifically the production of surface hydroxyl and carbon containing intermediates in the reforming process, by the scission of C-C and O-H bonds assisted by interaction between the metal and oxide support.

EXPERIMENTAL SECTION

AP-XPS studies were performed at the Advanced Light Source in Berkeley, CA (beamline 9.3.2). A VG Scienta R4000 HiPP analyzer was used for XPS analysis.[24] The O 1s region was probed with photon energy of 650 eV, and the C 1s, Ni 3p, and Ce 4d

regions with photon energy of 490 eV and a resolution of ~0.2 eV. The Ce 4d photoemission lines were used for binding energy calibration based on the 122.8 eV satellite features.[25] AP-IRRAS was performed in a combined UHV/elevated-pressure cell system with a Bruker IFS 66v/S spectrometer. Spectra were collected at a resolution of 4 cm^{-1} by using a grazing angle. The ethanol source (Pharmco-aaper, ACS/USP grade) was freeze-pumped-thawed in liquid nitrogen to remove gaseous contaminants.

Ce metal was evaporated onto a Ru single crystal (0001) held at 700 K in the presence of 5×10^{-7} Torr O_2, and then annealed to 800 K for 10 mins at the same O_2 pressure.[26] The ceria films were estimated to be ca. 4 nm thick (~10 layers of O-Ce-O) based on the attenuation of the Ru 3d XPS signal with 650 eV incident photo energy, which can eliminate the interference of Ru $3d_{3/2}$ (284.0 eV) to the C 1s signal. Ni was vapor deposited on the as-prepared ceria film at 300 K under vacuum and then annealed to 700 K for 1 min. Ni coverage calibration has been described elsewhere previously,[26] and the deposition rate of Ni was estimated to be ~0.15 ML/min. The Ni coverage in all experiments presented here are approximated to be 0.1~0.15 ML. Scanning tunneling microscopy (STM) studies show that the as-annealed Ni particles around this coverage are uniformly dispersed on the CeO_2(111) film with an average size of 2.7 nm width and 0.5 nm height.[26-27]

RESULTS and DISCUSSION

Ceria alone is not catalytically active for the ESR process, however hydrocarbon oxygenates such as ethanol and H_2O react with both Ce^{4+} and Ce^{3+}. Previously, studies in

ultra high vacuum (UHV) conditions have identified the ability of Ce^{3+} to dissociate H_2O to OH, while both Ce^{3+} and Ce^{4+} can produce ethoxy (CH_3CH_2O-) species through deprotonation. It has also been well established that ethanol is a strong reducing agent of ceria converting Ce^{4+} to Ce^{3+}, while water is a poor oxidant able to heal oxygen vacancies through the liberation of H_2.[28] We will start by unraveling the chemistry of ethanol and H_2O at elevated pressures over CeO_2(111).

1.1. Ethanol reaction on CeO_2(111)

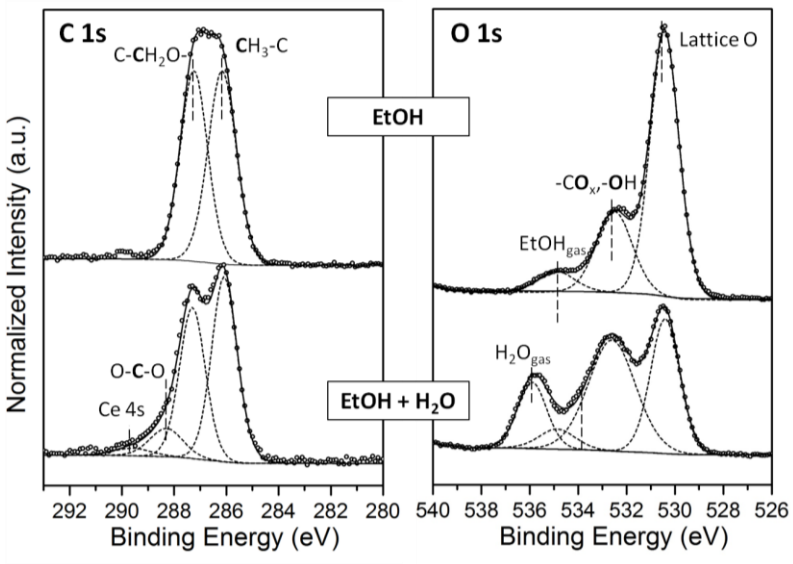

Figure 1. C 1s and O 1s spectra of the CeO_2(111) film under 40 mTorr of ethanol vapor at 300 K with/without adding H_2O (200 mTorr).

Figure 1 shows C 1s and O 1s AP-XP spectra obtained from the CeO_2(111) surface under a pressure of 40 mTorr of ethanol with and without adding 200 mTorr of H_2O at 300 K. With an exposure of 40 mTorr of ethanol, the C 1s region shows the formation of ethoxy species on the CeO_2(111) surface. The two peaks located at 287.2 eV

and 286.1 eV are attributed to the methylene (-**C**H_2-O-) and methyl carbon (-**C**H_3) in the ethoxy species, respectively.[15, 26, 29] In agreement with previous UHV studies of alcohol adsorption on CeO_2(111),[15, 26, 29-30] ethanol adsorbs dissociatively at 300 K, and no molecularly adsorbed ethanol is observed on the surface above room temperature. After mixing with 200 mTorr of water, a small shoulder appears along with the ethoxy features at a higher binding energy of 288.2 eV, and the relative intensity of the two ethoxy peaks changes. This indicates that even at room temperature some reaction occurs between the two reactants, which likely results in formation of a small amount of dioxyethylene species through a partial transition from the mono-dentate methylene carbon (CH_3**C**H_2-O-) of ethoxy to bi-dentate dioxy-carbon (CH_3**C**HO_2-) of dioxyethylene.[30-31]

In the O 1s region, before adding water, the spectrum can be fitted with the lattice oxygen from ceria at 530.4 eV, O from gas phase ethanol at 534.9 eV and another feature at 532.5 eV. This peak at 532.5 eV can be assigned to the O from ethoxy species as found in ethoxy (CH_3CH_2O-) and hydroxyl groups (-OH) that form upon binding of deprotonated H to lattice O of ceria due to the dissociative adsorption of ethanol. After adding another 200 mTorr of H_2O into the reaction to make a ~5:1 (H_2O/EtOH) vapor mixture, deconvolution of the spectrum shows an extra gas phase feature at 536.0 eV for 200 mTorr water vapor.[32-33] Moreover, the peak intensity of the ceria lattice O is significantly attenuated, which is mainly a result of the increased scattering of photoelectron due to the higher concentration of gas as well as surface adsorbed species between the ceria film and analyzer cone.

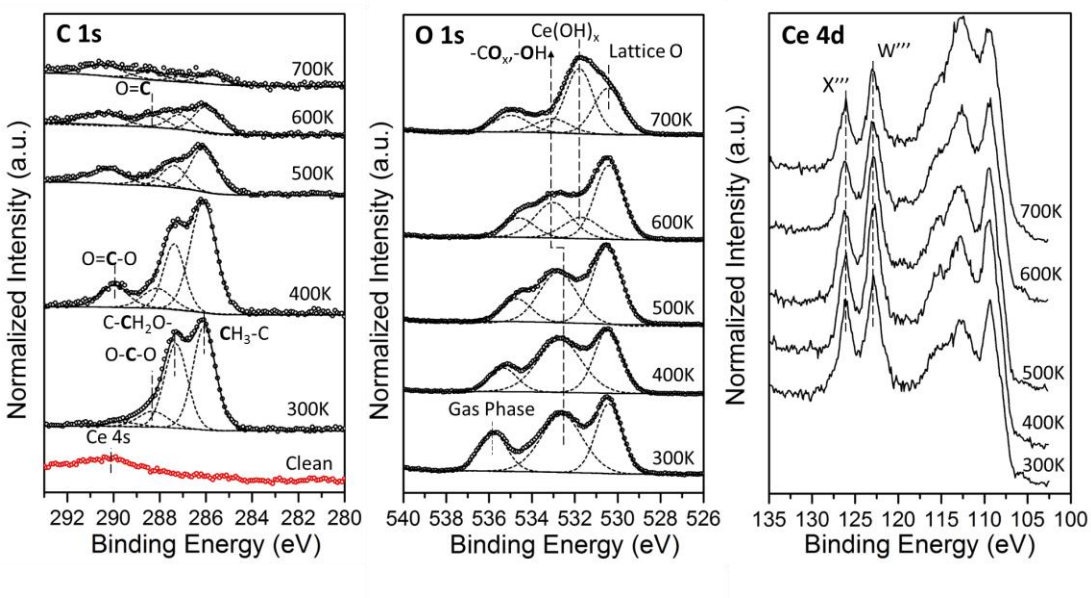

Figure 2. C 1s, O 1s and Ce 4d spectra for the CeO_2(111) surface under ethanol steam reforming conditions (40 mTorr ethanol + 200 mTorr H_2O).

The catalyst was then heated from 300 to 700 K by 100 K increments in an ambient of 40 mTorr ethanol and 200 mTorr H_2O, and the corresponding AP-XPS results for the C 1s, O 1s and Ce 4d regions are shown in Figure 2. In the C 1s spectra, the predominant ethoxy species at 287.2 eV and 286.1 eV gradually desorb from the surface up to 700 K. Furthermore, two additional features appear as a result of the increasing temperature at 288.2 and 289.8 eV. These two features can be attributed to dioxyethylene (CH_3CHO_2-) and acetates (C_2H_3OO-) species, respectively, and they occur as a consequence of the oxidation of ethoxy species.[31, 34] No additional carbon species are evident.

In the O 1s region, the most prevalent peak is that of the lattice O at 530.4 eV. The distinguishable fitting of the gas phase features, for ethanol and water was difficult

as these features change in both position and intensity under reaction conditions and temperatures. The changes of the gas phase peak has been observed previously,[35] and it is related to several factors including the changes in concentration of reactants and products, the work function at the near surface of the sample as well as variations of partial pressures of each gas. Therefore, considering the complexity of the gas mixture (reactants and products), we represent the gas phase feature with only one single broad peak. On the other hand, the broad peak at 532.5 eV that was previously assigned to –OH/ethoxy species gradually decreases in intensity from 500 K and shifts to a higher binding energy of 533.0 eV at 600 K. Taking into consideration that other hydrocarbon oxygenate species are present in the C 1s spectrum in addition to ethoxy at higher temperature, this region can have co-existence of species such as O-C-O from dioxyethylene[31] and the carboxylate oxygen (-COO) from acetate species,[34] that also appear in a similar region ~533.0 eV. The formation of these species is herein attributed to the further oxidation of ethoxy species. Furthermore, a new feature centered at 531.8 eV appears at 600 K and dominates at 700 K while the lattice oxygen appears considerably attenuated. Since most of the carbon species have desorbed by this temperature based on the C 1s spectrum, the peak at 531.8 eV cannot be assigned to any C-containing species. As will be discussed below, we tentatively assign this peak to the Ce(III) hydroxide ($Ce^{3+}(OH)_x$) formed in the hydroxyl-rich background.

By looking at the Ce 4d region in figure 2, the relative degree of reduction of the CeO_2(111) film can be identified by comparing the intensities of the peaks at 122.8 and 126.1 eV, labeled as X‴ and W‴, respectively.[25, 36] These two features are solely associated with Ce^{4+} spin−orbit splitting. Herein, one can observe that the CeO_2(111) film

has started to be reduced from 500 K to 700 K , and fitting of the Ce 4d spectrum at 700 K indicates that the surface of the ceria film consists of ~40% Ce^{3+}. Therefore the peak at 531.8 eV in the O 1s region could be assigned to either O from Ce_2O_3 or $Ce^{3+}(OH)_x$-like compound formed in the 240 mTorr of ethanol/H_2O vapor mixture. However, in previous studies of ceria surfaces by Mullins et al. and Matolin et al., the reported peak shift from CeO_2 to Ce_2O_3 is 0.3~0.8 eV.[25, 37] In our case, we observe a 1.4 eV shift from the lattice oxygen of CeO_2, a position that is in the range of reported hydroxide compounds.[38-39] Furthermore, in our previous study of the ceria film surface with the same extent of reduction (~40%),[26] no feature at 531.8 eV other than slight broadening of the lattice oxygen peak was evident. Thus, the assignment of this peak to Ce_2O_3 can be ruled out, and it is most likely $Ce^{3+}(OH)_x$ hydroxide that forms by hydroxylation of surface and subsurface layers of the film during the exposition of the highly reduced ceria surface to the 240 mTorr ethanol/water environment.

In the results discussed above, no evidence of C-C bond scission was observed, indicating that ceria alone is not likely to perform the most essential step in catalytically activating the ESR reaction, which is consistent with previous studies on both model and powder systems.[8, 26] However, ethanol does react with ceria to produce hydrocarbon oxygenates such as acetaldehyde, and ceria can be strongly reduced by ethanol to give rise to Ce^{3+} and its associated O vacancies. The creation of Ce^{3+} and O vacancies will in turn dissociate H_2O to –OH groups and even give rise to the formation of ceria hydroxide compounds. Furthermore, it is worth noting that despite the 1:5 ratio in favor a strongly oxidizing reactant mixture, the role of ethanol as a strong reducing agent is far greater than the oxidizing strength of water.

1.2. Ethanol reaction on Ni-CeO_2(111)

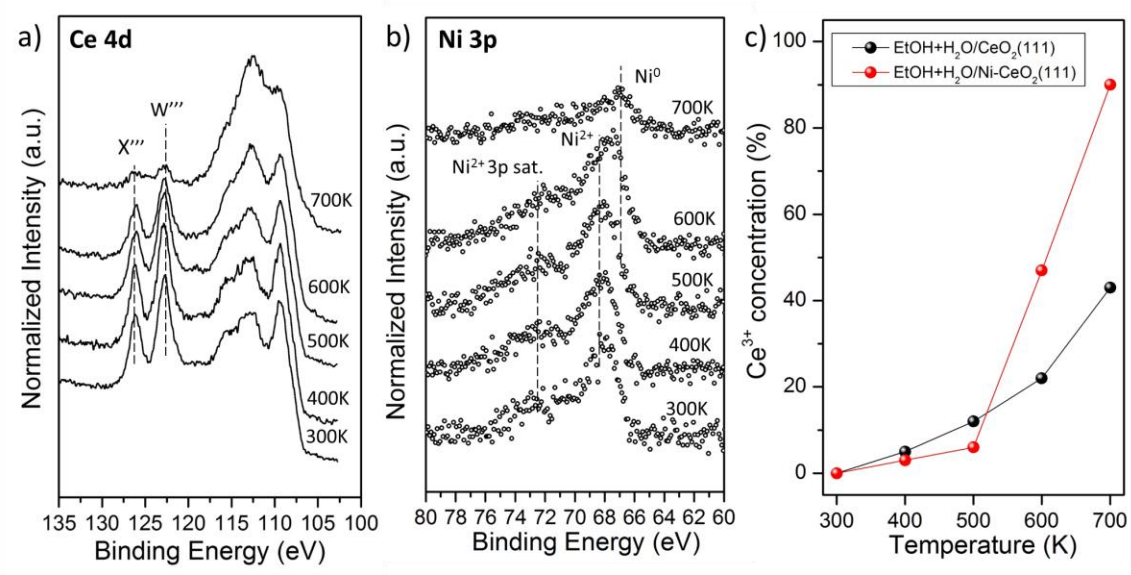

Figure 3. a,b) Ce 4d and Ni 3p spectra for the Ni-CeO_2(111) surface under ethanol steam reforming conditions (40 mTorr EtOH + 200 mTorr H_2O), c) Surface Ce^{3+} concentration comparison between CeO_2(111) and Ni-CeO_2(111) catalysts.

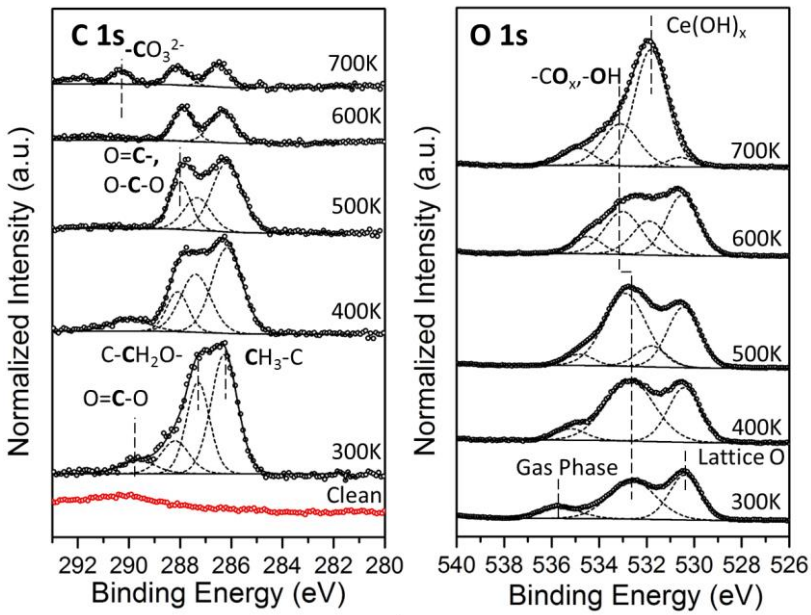

Figure 4. C 1s and O 1s spectra for the Ni-CeO_2(111) surface under ethanol steam reforming conditions (40 mTorr ethanol + 200 mTorr H_2O).

Having established the surface chemistry over CeO_2(111), we now turn to the role of Ni nanoparticles supported on CeO_2(111). From our previous studies we have established that the most catalytically active and stable Ni prevails at low coverage and low dimensionality, while maintaining good contact with the ceria support.[16, 21] Thus we investigated the ethanol reaction on Ni-CeO_2(111) surface with a small coverage of Ni ($\Theta_{Ni} \approx 0.15$ ML). Following the same procedure of experimentation as on the bare ceria film, 40 mTorr of ethanol and 200 mTorr of water were introduced into the chamber at 300 K and the surface was subsequently stepwise heated up to 700 K. First, the Ce 4d/Ni 3p regions of AP-XPS results are presented in figure 3a and b. The Ni nanoparticles initially remain as Ni^{2+} on CeO_2(111) at 300 K, in agreement with our previous study of Ni deposition on ceria.[26, 40] Upon heating to 700 K, nearly all of the Ce^{4+} contributions in the Ce 4d spectrum disappeared, and simultaneously the supported NiO nanoparticles are reduced to metallic Ni as evident in the Ni 3p region. The reduction extent derived from Ce 4d spectra with/without Ni deposition is also compared in figure 3c. In contrast with the bare ceria film, the ~90% reduction of the Ni-CeO_2(111) film demonstrates that the top few layers of the catalyst are almost completely reduced to Ce^{3+} under the steam reforming conditions. This reduction is likely due to several effects, including the ability of Ni and ceria to dissociate H_2O, the strong interaction between Ni and ceria, and a possible strain in the ceria due to doping with Ni, which can make oxide lattice favor the formation of Ce^{3+} and O vacancies.[16, 21]

For the surface species evolution, figure 4 depicts the C 1s/O 1s AP-XPS results for the heated surface. In the C 1s spectra, starting from 300 K, a small amount of acetate (289.8 eV) as well as dioxyethylene species (288.2 eV) are formed along with the ethoxy species (287.2 eV and 286.1 eV), which matches the results from the bare ceria film. However, the difference in ethanol reaction between Ni-CeO_2(111) and the CeO_2(111) film becomes apparent when heating up to 700 K. A peak at 290.3 eV indicative of carbonate groups is observed, revealing that the C-C bond cleavage has occurred along with further oxidation to carbonates (-CO_3^{2-}).[41-44] The formation of carbonates was not seen in our previous UHV study of ethanol adsorption on Ni-CeO_2(111) likely due to the low pressure of ethanol/water, not sufficient oxidative environment to give rise to the complete oxidation from hydrocarbon to carbonate (CO_3^{2-}). Similarly, in the O 1s region, peaks can be clearly seen for lattice O of ceria (530.4 eV) and gas phase mixture of water/ethanol (535.9 eV) at 300 K. Analogous to the reaction on the bare ceria film and considering the complexity of having multiple surface species, a broad peak (fwhm=2.1 eV) centered at 532.5 eV can be identified, representing a combination of surface hydroxyl and hydrocarbon oxygenate related species (eg. surface ethoxy, dioxyethylene and acetate, etc.). Upon heating to 700 K, this peak attenuates and shifts to 533.2 eV, as a result of the development of surface hydroxyl/ethoxy to more oxidative species. Moreover, the lattice oxygen peak of CeO_2 appears attenuated and has nearly vanished by 700 K, while a peak at 531.8 eV, similar to the one observed on bare ceria film, emerges at 500 K and finally dominates at 700 K. This again suggests the formation of a hydroxide compound. Recalling that a heavy reduction of the top layers of Ni-CeO_2(111) film occurred as shown in figure 3c, one can conclude that the extent of hydroxylation

and concentration of ceria hydroxide layers is much more significant compared to the bare ceria, as practically all the lattice O signal from the CeO_2(111) film has been covered. Additionally, we have attempted to ascertain the extent of the surface hydroxide formation by XPS depth profiling of this surface (see figure S1). The oxygen species from multiple layers of CeO_2(111) film were probed with varying incident photon energy (550-850 eV), tuning the escape depth of photoelectrons from the O 1s core level, elucidating the location of Ce^{3+} and OH species within the first few layers of the ceria film. The richest zone of OH and Ce^{3+} species appears approximately in the top 1 nm, or ~3-4 atomic monolayers of O-Ce-O of this surface. This provides complementary information about the surface state of Ni-CeO_x catalysts, in comparison to previous powder catalysts where we only elucidated the bulk state of the catalyst and ascertained less than 30% of the bulk to have undergone reduction.[8, 45] These results suggest that the first few surface layers are not only reduced but remain hydroxylated with a high dispersion of small Ni nanoparticles.

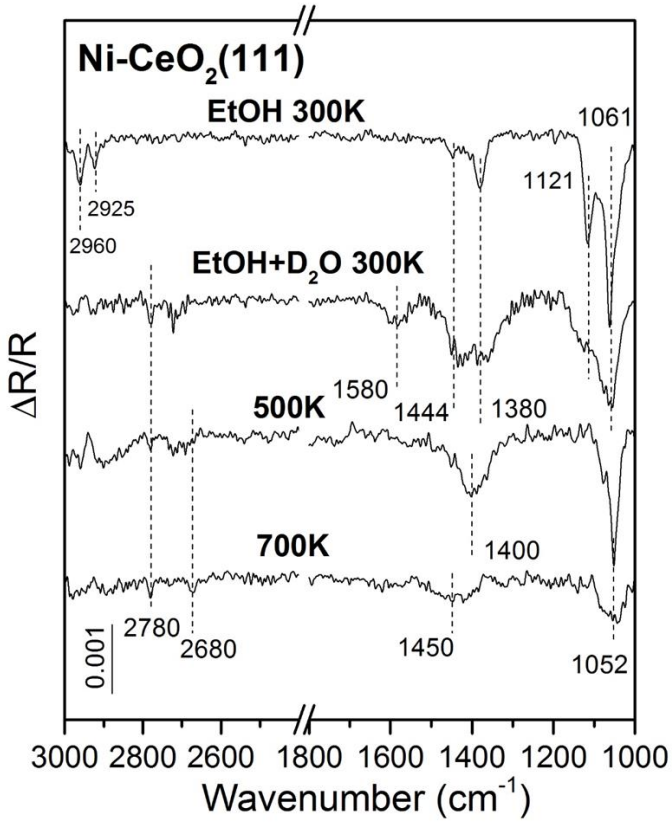

Figure 5. AP-IRRAS spectra for the Ni-CeO_2(111) surface under ethanol steam reforming conditions (10 mTorr ethanol + 40 mTorr D_2O).

The AP-IRRAS results under similar reaction conditions further confirm the surface species observed in AP-XPS experiments, as shown in figure 5. With only ethanol, characteristic infrared peaks for ethoxy species are identified on the Ni-CeO_2(111) film by the CO bands at 1121 cm^{-1} for monodentate ν(CO) and at 1061 cm^{-1} for bidentate ν(CO) or ρ(CH_3), whereas the CH stretching bands are found at 2960 cm-1 and 2925 cm^{-1} for $\nu_{as}(CH_3)$ and $\nu_{as}(CH_2)$, respectively.[46] Moreover, the peaks at 1444 and 1380 cm^{-1} are assigned to the bending mode of δ(CH_2) and δ(CH_3). After adding water (D_2O), significant changes were observed compared to the surface with pure ethanol. A water gas phase peak at 2780 cm^{-1} shows up, while the regions at 1350-1450 cm^{-1} and

1050-1150 cm^{-1} become broad and not well resolved, probably due to the co-existence of multiple bands from ethoxy species and other hydrocarbon oxygenates (acetate/dioxyethylene). A new peak that is indicative of the ν_{as}(COO) band from acetate species emerged at 1580 cm^{-1}, in agreement with the AP-XPS observation in figure 4. Upon an increase of the temperature up to 700 K, the nearly disappearance of CH_x stretching bands region at ~2900 cm^{-1} suggests the dehydrogenation of CH_x surface species to produce hydrogen, while a broad hump centered at 1450 cm^{-1} is attributed to the small amount of carbonate species, as also observed in the 700 K C 1s spectrum in figure 4.[47] Compared with previous Diffuse Reflectance Infrared Fourier Transform Spectroscopy (DRIFTS) study of powder Ni-CeO_2,[8] the formation of acetates species at room temperature and its subsequent transformation to carbonates species at higher temperature are evident in both cases, but the all the features on the powder system are more pronounced and could be retained at higher temperature, probably due to the multiple crystal facets of powder ceria affect the adsorption/desorption selectivity. In addition, a small peak at 2680 cm^{-1} corresponding to the ν(OD) derived from the dissociation of D_2O, is resolved at 700 K.[48] Correlating this with the $Ce(OH)_x$ demonstrated in the AP-XPS results above, the observation of hydroxyls (-OD) verifies the participation of water in the formation of ceria hydroxides while water can be the hydroxyl feed stock for the reforming reaction.

Thus, combining data of ambient pressure XPS and IRRAS, it is clear that Ni-CeO_2(111) is active for ethanol steam reforming at ~700 K compared with the bare ceria film surfaces. Also note that Ni nanoparticles are present as metallic Ni^0, on the highly reduced and hydroxylated ceria surface, indicating that the active phase for ethanol steam

reforming includes both metallic Ni and $Ce^{3+}(OH)_x$. Nevertheless, how these two components correlate with each other and their roles in the steam reforming reaction under steady state conditions is not obvious. Therefore, we performed additional experiments, initially exposing the surface to ethanol and then sequentially adding water at 700 K, while the catalyst is at its most active state, as will be discussed below.

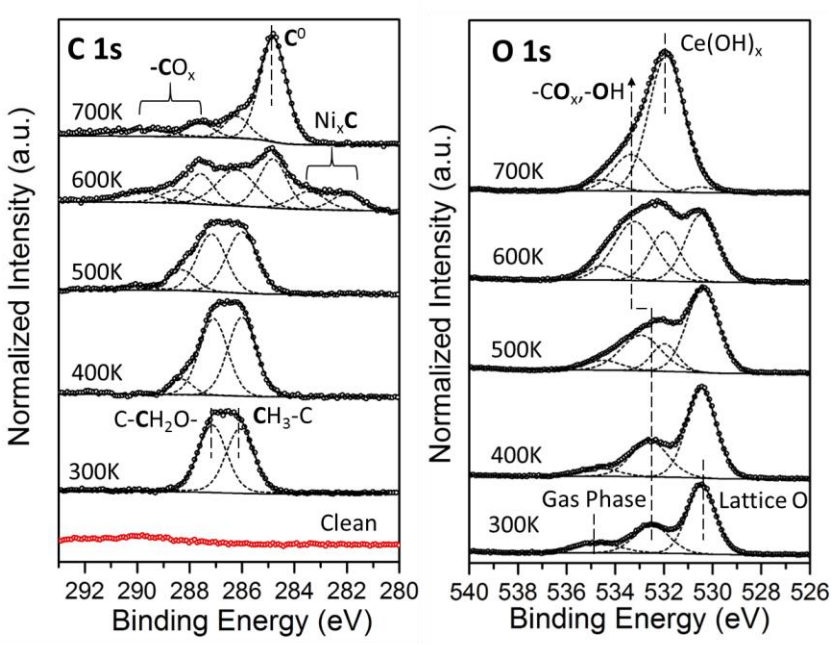

Figure 6. C 1s and O 1s spectra for the Ni-CeO_2(111) surface under a background of 40 mTorr ethanol at elevated temperature from 300-700 K.

On a freshly prepared surface with similar coverage of Ni ($\Theta_{Ni} \approx 0.12$ ML), the sample was stepwise heated in the presence of 40 mTorr of ethanol. As observed previously, the surface was drastically reduced from 600 K onwards, and metallic Ni was formed (see figure S2). The corresponding O 1s/C 1s spectra are shown in figure 6. The most important difference with respect to the ethanol steam reforming reaction in figure 4 are the C 1s spectra above 600 K. In the absence of water, the reaction gave rise to a very

complex C 1s spectrum where numerous surface species formed simultaneously as a transition state by 600 K. The peaks appearing from 288.0 eV to 290.0 eV are attributed to carbon oxygenates species (-CO_x) as indicated in figure 6, probably bound to several parts of the Ni and ceria components. More importantly, at binding energy below 285.0 eV, three new features associated with non-oxygenated carbon appeared at 284.8 eV, 283.4 eV and 282.0 eV. The one at 284.8 eV is assigned to surface carbon (C^0), indicating that coke formation occurred on the surface, while the other two are attributed to the formation of nickel carbide species (Ni_3C/Ni_xC).[26, 49] Nickel carbides species were similarly observed in our previous study of both power and model Ni-CeO_2 systems.[8, 26] It is also reported as a precursor for the growth of graphene on nickel.[50-51] Nickel carbides are metastable and will further decompose into metallic Ni and surface carbon (coke) by 733 K.[52] Herein, a more prominent surface carbon feature at 284.8 eV formed at 700 K as evident in the C 1s spectra, which confirms the importance of metallic nickel, as the active agent responsible for C-C and C-H bond breaking in the decomposition of ethoxy related intermediates. Moreover, this experiment reveals that metallic nickel is also responsible for the surface carbon accumulation and that it can drive the reaction to an unselective reaction pathway in an ethanol rich reactant stream. The chemistry of water and OH formation in the ESR reaction, appears to be pivotal, and may lead to the protection of the active sites and mitigate deactivation.[1]

To gain further insights into the effect of water and its associated hydroxyl groups on the reaction in an *in situ* manner, we sequentially introduced 200 mTorr of water into the ethanol ambient while the surface was kept at 700 K, as shown in figure 7. In the C 1s spectra, the instant decrease of the intensity of the surface carbon peak at 284.8 eV upon

the introduction of water is evident, whereas the intensity of the carbon oxygenates related peaks (288.0 eV- 289.0 eV) increased, clearly demonstrating the oxidation process through the complete dissociation of H_2O and incorporation of O. This is also evident in the O 1s region as the enlarged peak at 533.2 eV for carbonate/carboxylates species after addition of water, indicating the re-oxidation of the surface carbon species. This result reveals that water and its associated hydroxyl groups play a vital role in assisting the removal of surface carbon. Intuitively based on this, the H_2 liberated from each molecule of water associated with the oxidation is also potentially a major contributor towards the yield of H_2 in the overall mass balance of the reaction.

Previous studies have identified that the formation of hydroxyl groups is favored on reduced ceria,[28] and these hydroxyl groups are likely to impart a strong interaction with the oxide supported metal particles.[53] Additionally, Ni/Ni^{2+} on the $CeO_x(111)$ substrate can also readily dissociate water to form hydroxyls on the surface.[21] Furthermore, our earlier isotope study of the reaction of ethanol on the $Ni\text{-}CeO_x(111)$ surface under UHV showed that there is oxygen transfer between ceria and surface carbon on Ni nanoparticles, and a significant amount of D_2 and CO are produced in the temperature programmed desorption (TPD) data after introducing D_2O into the reaction.[26] Herewith, considering all the factors mentioned above and also noting that top few layers of the ceria film was fully reduced and hydroxylated at 700 K, this *in situ* observation of oxidation and coke removal by addition of 200 mTorr of water reveals that, under steady state reforming conditions, the oxygen or hydroxyl transfer between water and surface carbon occurs in the form of hydroxyls and it could go through ceria hydroxide as a possible intermediate. Moreover, the existence of metal-support interactions between Ni

and ceria after depositing very small amount of Ni (Θ_{Ni} < 0.15 ML) could further facilitate this oxygen transfer.[16, 21] Therefore, the possible mechanistic pathway on Ni-Ceria could be interpreted as:

On Ceria sites:

$CH_3CH_2OH \rightarrow CH_3CH_2O$ (ad) + H(ad);

$H_2O \rightarrow OH(ad) + H(ad)$;

$CH_3CH_2O(ad) + OH/O(lattice) \rightarrow C_2O_xH_y$ (eg. CH_3COO-) + nH(ad);

$2H(ad) \rightarrow H_2$ (gas)

On Ni sites or Ce-Ni interfaces:

$C_2O_xH_y \rightarrow CO_x(ad) + CH_y(ad)$;

CO_x (ad) $\rightarrow CO/CO_2$ (gas);

$CH_y + xOH(ad) \rightarrow CO/CO_2 + (x+y)H(ad)$ and $2H(ad) \rightarrow H_2$ (gas)

Coking process: $2CO \rightarrow$ C (or coke) + CO_2 or $CH_y \rightarrow$ C (or coke) + yH(ad);

On the other hand, the reappearance of nickel carbide species (Ni_3C/Ni_xC) after introducing water in the C 1s spectra of figure 7 points at a possible re-oxidation pathway of surface carbon through a strong interaction with Ni:

$OH(ad) + xNi^0 + coke \rightarrow HO\text{-}Ni_xC \rightarrow xNi^0 + CO/CO_2 + H(ad)$

Thus, under steady state reaction conditions, it is likely that two competing processes will take place on the surface: 1. the accumulation of coke due to C-C/C-H bond cleavage by metallic Ni and 2. the re-oxidation of surface carbon by hydroxyls provided by the interaction between water and ceria in the form of $Ce^{3+}(OH)_x$. More importantly, the redox property of the oxides as well as the synergistic interplay between ceria and low loading of Ni are crucial in order to sustain the stability and selectivity of the reaction by facilitating the oxygen transfer from water to ceria and then to surface carbon on nickel nanoparticles.

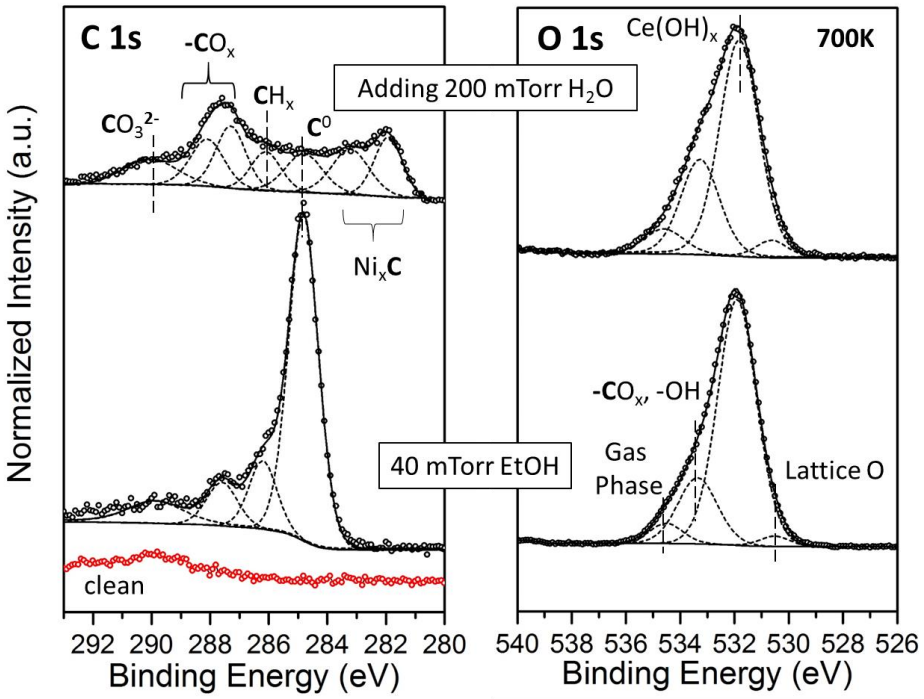

Figure 7. C 1s and O 1s spectra for the Ni-CeO_2(111) surface under a background of 40 mTorr ethanol at 700 K before and after adding another 200 mTorr of water.

CONCLUSIONS

We have studied the steam reforming of ethanol over a Ni-CeO_2(111) catalyst with a combination of *in situ* AP-XPS and AP-IRRAS. The layers near the surface of the ceria substrate stay highly reduced and hydroxylated as $Ce^{3+}(OH)_x$, and the doping of small amount of Ni nanoparticles enhances this effect. Under reaction conditions, metallic Ni is the active phase leading to both C-C and C-H cleavages of ethanol as well as the carbon accumulation or coking, while reduced ceria assists the deprotonation of ethanol and water with subsequent generation of hydroxyls which are crucial for the further reaction with CH_x or coke. The *in situ* observation of coke formation/removal from AP-XPS results gives an important insight into the stability and selectivity of the catalyst: The accumulation of surface carbon can be mitigated by the co-existence and cooperative interplay of small Ni^0 particles and $Ce^{3+}(OH)_x$, facilitating hydroxyls/oxygen transfer through a strong metal-support interaction.

AUTHOR INFORMATION

Corresponding Author Email: ssenanay@bnl.gov

NOTES

The authors declare no competing financial interest.

ASSOCIATED CONTENT

The Supporting Information is available free of charge on the ACS Publications website. Figure S1: O1s data as a function of incident photon energy. Figure S2: Ce 4d and Ni 3p spectra upon ethanol exposure.

ACKNOWLEDGMENT

The research carried out at Brookhaven National Laboratory, was supported by the U.S. Department of Energy, Office of Science and Office of Basic Energy Sciences under contract No. DE-SC0012704. The collaborative work with Charles University in Prague, is part of the KONTAKT project that was supported by the Ministry of Education of the Czech Republic (LH15272). The Advanced Light Source is supported by the Director, Office of Science, Office of Basic Energy Sciences, of the U.S. Department of Energy under Contract No. DE-AC02-05CH11231.

References

(1) Mattos, L. V.; Jacobs, G.; Davis, B. H.; Noronha, F. B. *Chem. Rev.* **2012**, *112*, 4094-4123.
(2) Huber, G. W.; Iborra, S.; Corma, A. *Chem. Rev.* **2006**, *106*, 4044-4098.
(3) Piscina, P. R. d. l.; Homs, N. *Chem. Soc. Rev.* **2008**, *37*, 2459-2467.
(4) Llorca, J.; Homs, N. s.; Sales, J.; de la Piscina, P. R. r. *J. Catal.* **2002**, *209*, 306-317.
(5) Palma, V.; Castaldo, F.; Ciambelli, P.; Iaquaniello, G. *Appl. Catal. B* **2014**, *145*, 73-84.
(6) Soykal, I. I.; Sohn, H.; Singh, D.; Miller, J. T.; Ozkan, U. S. *ACS Catalysis* **2014**, *4*, 585-592.
(7) Aupretre, F.; Descorme, C.; Duprez, D.; Casanave, D.; Uzio, D. *J. Catal.* **2005**, *233*, 464-477.
(8) Xu, W.; Liu, Z.; Johnston-Peck, A. C.; Senanayake, S. D.; Zhou, G.; Stacchiola, D.; Stach, E. A.; Rodriguez, J. A. *ACS Catalysis* **2013**, *3*, 975-984.
(9) Sheng, P. Y.; Bowmaker, G. A.; Idriss, H. *Appl. Catal. A* **2004**, *261*, 171-181.
(10) Ciambelli, P.; Palma, V.; Ruggiero, A. *Appl. Catal. B* **2010**, *96*, 18-27.
(11) Liguras, D. K.; Kondarides, D. I.; Verykios, X. E. *Appl. Catal. B* **2003**, *43*, 345-354.
(12) Zhang, B.; Tang, X.; Li, Y.; Cai, W.; Xu, Y.; Shen, W. *Catal. Commun.* **2006**, *7*, 367-372.
(13) Roh, H.-S.; Platon, A.; Wang, Y.; King, D. L. *Catal. Lett.* **2006**, *110*, 1-6.
(14) Alberton, A. L.; Souza, M. M. V. M.; Schmal, M. *Catal. Today* **2007**, *123*, 257-264.
(15) Senanayake, S. D.; Mudiyanselage, K.; Bruix, A.; Agnoli, S.; Hrbek, J.; Stacchiola, D.; Rodriguez, J. A. *J. Phys. Chem. C* **2014**, *118*, 25057-25064.
(16) Zhou, G.; Barrio, L.; Agnoli, S.; Senanayake, S. D.; Evans, J.; Kubacka, A.; Estrella, M.; Hanson, J. C.; Martínez-Arias, A.; Fernández-García, M.; Rodriguez, J. A. *Angew. Chem.* **2010**, *122*, 9874-9878.
(17) Frusteri, F.; Freni, S.; Spadaro, L.; Chiodo, V.; Bonura, G.; Donato, S.; Cavallaro, S. *Catal. Commun.* **2004**, *5*, 611-615.
(18) Breen, J. P.; Burch, R.; Coleman, H. M. *Appl. Catal. B* **2002**, *39*, 65-74.
(19) Carrasco, J.; Barrio, L.; Liu, P.; Rodriguez, J. A.; Ganduglia-Pirovano, M. V. *J. Phys. Chem. C* **2013**, *117*, 8241-8250.
(20) Senanayake, S. D.; Evans, J.; Agnoli, S.; Barrio, L.; Chen, T.-L.; Hrbek, J.; Rodriguez, J. A. *Top. Catal.* **2011**, *54*, 34-41.
(21) Carrasco, J.; López-Durán, D.; Liu, Z.; Duchoň, T.; Evans, J.; Senanayake, S. D.; Crumlin, E. J.; Matolín, V.; Rodríguez, J. A.; Ganduglia-Pirovano, M. V. *Angew. Chem. Int. Ed.* **2015**, *54*, 3917-3921.

(22) Pirez, C.; Capron, M.; Jobic, H.; Dumeignil, F.; Jalowiecki-Duhamel, L. *Angew. Chem. Int. Ed.* **2011**, *50*, 10193-10197.
(23) Jalowiecki-Duhamel, L.; Pirez, C.; Capron, M.; Dumeignil, F.; Payen, E. *Int. J. Hydrogen Energy* **2010**, *35*, 12741-12750.
(24) Grass, M. E.; Karlsson, P. G.; Aksoy, F.; Lundqvist, M.; Wannberg, B.; Mun, B. S.; Hussain, Z.; Liu, Z. *Rev. Sci. Instrum.* **2010**, *81*, 053106.
(25) Mullins, D.; Overbury, S.; Huntley, D. *Surf. Sci.* **1998**, *409*, 307-319.
(26) Liu, Z.; Duchoň, T.; Wang, H.; Peterson, E. W.; Zhou, Y.; Luo, S.; Zhou, J.; Matolín, V.; Stacchiola, D. J.; Rodriguez, J. A.; Senanayake, S. D. *J. Phys. Chem. C* **2015**, *119*, 18248-18256.
(27) Zhou, Y.; Zhou, J. *J. Phys. Chem. C* **2012**, *116*, 9544-9549.
(28) Mullins, D. R.; Albrecht, P. M.; Chen, T.-L.; Calaza, F. C.; Biegalski, M. D.; Christen, H. M.; Overbury, S. H. *J. Phys. Chem. C* **2012**, *116*, 19419-19428.
(29) Mullins, D. R.; Senanayake, S. D.; Chen, T. L. *J. Phys. Chem. C* **2010**, *114*, 17112-17119.
(30) Mullins, D. R.; Robbins, M. D.; Zhou, J. *Surf. Sci.* **2006**, *600*, 1547-1558.
(31) Mullins, D. R.; Albrecht, P. M. *J. Phys. Chem. C* **2013**, *117*, 14692-14700.
(32) Mudiyanselage, K.; Senanayake, S. D.; Feria, L.; Kundu, S.; Baber, A. E.; Graciani, J.; Vidal, A. B.; Agnoli, S.; Evans, J.; Chang, R.; Axnanda, S.; Liu, Z.; Sanz, J. F.; Liu, P.; Rodriguez, J. A.; Stacchiola, D. J. *Angew. Chem. Int. Ed.* **2013**, *52*, 5101-5105.
(33) Ketteler, G.; Yamamoto, S.; Bluhm, H.; Andersson, K.; Starr, D. E.; Ogletree, D. F.; Ogasawara, H.; Nilsson, A.; Salmeron, M. *J. Phys. Chem. C* **2007**, *111*, 8278-8282.
(34) Calaza, F. C.; Chen, T.-L.; Mullins, D. R.; Xu, Y.; Overbury, S. H. *Catal. Today* **2015**, *253*, 65-76.
(35) Axnanda, S.; Scheele, M.; Crumlin, E.; Mao, B.; Chang, R.; Rani, S.; Faiz, M.; Wang, S.; Alivisatos, A. P.; Liu, Z. *Nano Lett.* **2013**, *13*, 6176-6182.
(36) Mullins, D. R.; Radulovic, P. V.; Overbury, S. H. *Surf. Sci.* **1999**, *429*, 186-198.
(37) Duchoň, T.; Dvořák, F.; Aulická, M.; Stetsovych, V.; Vorokhta, M.; Mazur, D.; Veltruská, K.; Skála, T.; Mysliveček, J.; Matolínová, I.; Matolín, V. *J. Phys. Chem. C* **2014**, *118*, 357-365.
(38) Casella, I. G.; Guascito, M. R.; Sannazzaro, M. G. *J. Electroanal. Chem.* **1999**, *462*, 202-210.
(39) Mora, N.; Cano, E.; Polo, J. L.; Puente, J. M.; Bastidas, J. M. *Corros. Sci.* **2004**, *46*, 563-578.
(40) Zhou, Y.; Perket, J. M.; Zhou, J. *J. Phys. Chem. C* **2010**, *114*, 11853-11860.
(41) Neitzel, A.; Lykhach, Y.; Johánek, V.; Tsud, N.; Skála, T.; Prince, K. C.; Matolín, V.; Libuda, J. *J. Phys. Chem. C* **2015**, *119*, 13721-13734.
(42) Albrecht, P. M.; Jiang, D.-e.; Mullins, D. R. *J. Phys. Chem. C* **2014**, *118*, 9042-9050.
(43) Senanayake, S. D.; Mullins, D. R. *J. Phys. Chem. C* **2008**, *112*, 9744-9752.
(44) Senanayake, S. D.; Stacchiola, D.; Liu, P.; Mullins, C. B.; Hrbek, J.; Rodriguez, J. A. *J. Phys. Chem. C* **2009**, *113*, 19536-19544.
(45) Liu, Z.; Xu, W.; Yao, S.; Johnson-Peck, A. C.; Zhao, F.; Michorczyk, P.; Kubacka, A.; Stach, E. A.; Fernández-García, M.; Senanayake, S. D.; Rodriguez, J. A. *J. Catal.* **2015**, *321*, 90-99.
(46) Yee, A.; Morrison, S. J.; Idriss, H. *J. Catal.* **1999**, *186*, 279-295.
(47) Li, C.; Sakata, Y.; Arai, T.; Domen, K.; Maruya, K.-i.; Onishi, T. *J. Chem. Soc., Faraday Trans. 1* **1989**, *85*, 929-943.
(48) Mudiyanselage, K.; Senanayake, S. D.; Ramirez, P. J.; Kundu, S.; Baber, A.; Yang, F.; Agnoli, S.; Axnanda, S.; Liu, Z.; Hrbek, J.; Evans, J.; Rodriguez, J. A.; Stacchiola, D. *Top. Catal.* **2015**, *58*, 271-280.
(49) Czekaj, I.; Loviat, F.; Raimondi, F.; Wambach, J.; Biollaz, S.; Wokaun, A. *Appl. Catal. A* **2007**, *329*, 68-78.
(50) Rameshan, R.; Mayr, L.; Klötzer, B.; Eder, D.; Knop-Gericke, A.; Hävecker, M.; Blume, R.; Schlögl, R.; Zemlyanov, D. Y.; Penner, S. *J. Phys. Chem. C* **2015**, 119, 26948-26958.

(51) Weatherup, R. S.; D'Arsié, L.; Cabrero-Vilatela, A.; Caneva, S.; Blume, R.; Robertson, J.; Schloegl, R.; Hofmann, S. *J. Am. Chem. Soc.* **2015**, *137*, 14358-14366.
(52) Tanaka, T.; Ishihara, K. N.; Shingu, P. H. *Metall. Trans. A* **1992**, *23*, 2431-2435.
(53) Addou, R.; Senftle, T. P.; O'Connor, N.; Janik, M. J.; van Duin, A. C. T.; Batzill, M. *ACS Nano* **2014**, *8*, 6321-6333.